JACS
JOURNAL OF THE AMERICAN CHEMICAL SOCIETY
pubs.acs.org/JACS
Article

Closing the "One Monomer–Two Polymers–One Monomer" Loop via Orthogonal (De)polymerization of a Lactone/Olefin Hybrid

Changxia Shi, Ryan W. Clarke, Michael L. McGraw, and Eugene Y.-X. Chen*

Cite This: J. Am. Chem. Soc. 2022, 144, 2264–2275
Read Online
ACCESS | Metrics & More | Article Recommendations | Supporting Information

ABSTRACT: Two well-known low-ceiling-temperature (LCT) monomers, γ-butyrolactone (γ-BL) toward ring-opening polymerization (ROP) to polyester and cyclohexene toward ring-opening metathesis polymerization (ROMP) to poly(cyclic olefin), are notoriously "nonpolymerizable". Here we present a strategy to render not only polymerizability of both the γ-BL and cyclohexene sites, orthogonally, but also complete and orthogonal depolymerization, through creating an LCT/LCT hybrid, bicyclic lactone/olefin (BiL$^{=}$). This hybrid monomer undergoes orthogonal polymerization between ROP and ROMP, depending on the catalyst employed, affording two totally different classes of polymeric materials from this single monomer: polyester P(BiL$^{=}$)$_{ROP}$ via ROP and functionalized poly(cyclic olefin) P(BiL$^{=}$)$_{ROMP}$ via ROMP. Intriguingly, both P(BiL$^{=}$)$_{ROP}$ and P(BiL$^{=}$)$_{ROMP}$ are thermally robust but chemically recyclable under mild conditions (25–40 °C), in the presence of a catalyst, to recover cleanly the same monomer via chain unzipping and scission, respectively. In the ROP, topological and stereochemical controls have been achieved and the structures characterized. Furthermore, the intact functional group during the orthogonal polymerization (i.e., the double bond in ROP and the lactone in ROMP) is utilized for postfunctionalization for tuning materials' thermal and mechanical performances. The impressive depolymerization orthogonality further endows selective depolymerization of both the ROP/ROMP copolymer and the physical blend composites into the same starting monomer.

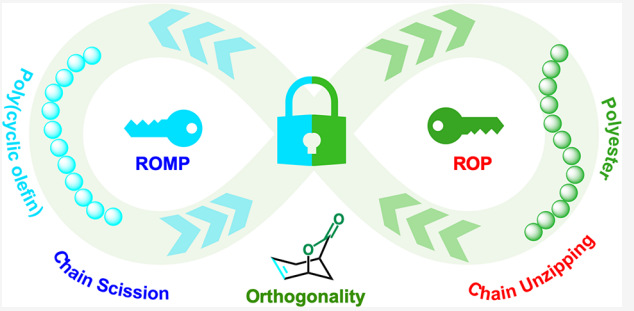

INTRODUCTION

As part of large worldwide efforts[1−14] combating the worsening plastics problem that has already caused not only plastics pollution crisis but also tremendous energy and materials value loss in the economy,[15−20] the development of next-generation, chemically recyclable polymers[21−31] represents one of the approaches addressing these complex issues.[32−34] However, redesign of tomorrow's polymers with chemical recyclability or biodegradability must consider not only their closed-loop life cycles but also their performance properties.[35,36] The strategy starts from monomer design[36−38]—the key to discovering new intrinsically circular polymers. The monomer is specifically designed to overcome typical trade-offs between monomer's polymerization/depolymerization thermodynamics and recyclability as well as material performance.[36] As this design is required to meet stringent thermodynamic, kinetic, and real-world performance requirements for ultimately developing circular plastics that exhibit not only full chemical recyclability but also high-performance properties, it still presents a formidable challenge.

With increasing demands for diverse polymer applications, effective methods have been developed to manipulate comonomer composition, topology, and functionality for targeted specific properties.[39] While well-established synthetic techniques exist for the facile and precision synthesis of conventional/nondegradable polymers, the same methodologies are rare in the realm of degradable/recyclable polymers where a higher level thermodynamic and chemoselection challenges persist.[40,41] Among several strategies, the ring-opening polymerization (ROP) of functional cyclic monomers is an effective approach to synthesize well-defined degradable/recyclable materials with excellent control over topology, tacticity, and sequence, and so on.[42−44] In this context, tremendous progress has recently been made in developing various classes of degradable/recyclable functional polymers[44,45] such as polyesters,[46−53] poly(ester–amide)s,[54] polythioesters,[55−57] and polycarbonates.[58−60] In spite of these advances, many synthetic approaches suffer from challenges arising from multistep routes for the synthesis of monomers[40] and the sensitivity of catalytic systems.[7] Additionally, the introduction of complexities, such as functional groups, often significantly decreases the recyclability of the

Received: November 21, 2021
Published: January 27, 2022

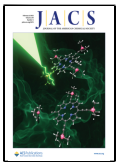

https://doi.org/10.1021/jacs.1c12278
J. Am. Chem. Soc. 2022, 144, 2264–2275

Scheme 1. Closing the "One Monomer−Two Polymers−One Monomer" Loop by LCT/LCT Hybrid Monomer Design to Bifunctional Lactone/Olefin Monomer BiL$^{=}$ That Exhibits Orthogonal Polymerizability between ROP and ROMP, Leading to Recyclable Polyester and Poly(cyclic olefin), Respectively[a]

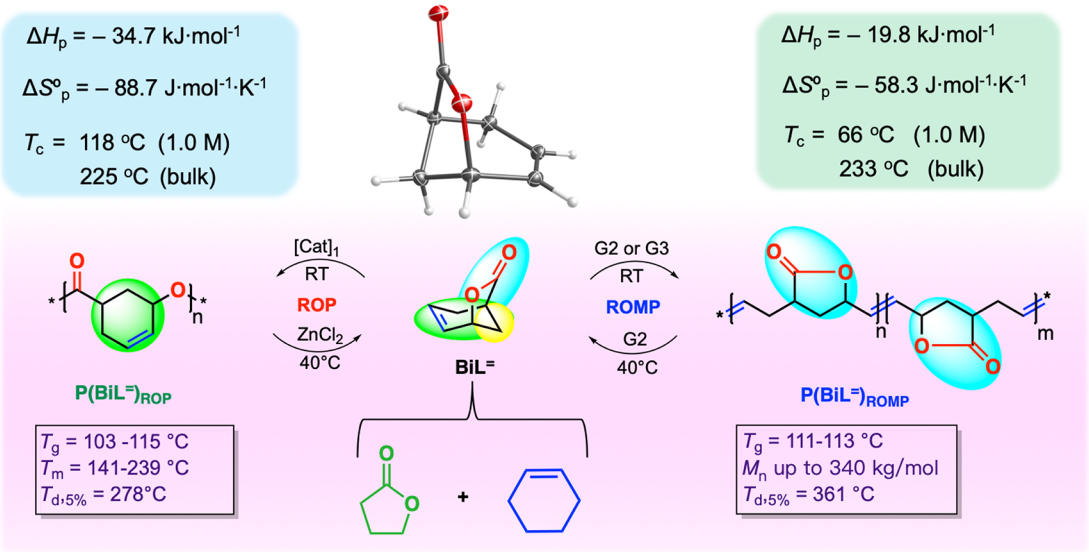

[a]Ceiling, glass-transition, melting-transition, and decomposition (at 5% weight loss) temperatures are denoted as T_c, T_g, T_m, and $T_{d,5\%}$, respectively.

polymer. With this in mind, the strategies that allow high levels of topological and functional group tolerance must be compatibilized with the strategies that allow recyclability.

Ring-opening metathesis polymerization (ROMP)[61−65] is a powerful method for preparing diverse poly(cyclic olefin)s. Strained cycloalkenes, such as norbornene and cyclooctene, are highly polymerizable because thermodynamics of their ring-opening favor polymerization over depolymerization and thus have been frequently used as monomers for poly(cyclic olefin) synthesis. Most recently, Wang et al. redesigned a cyclooctene monomer by transfusing a cyclobutane ring and successfully rendered (de)polymerization reversibility of the otherwise nonreversible, highly strained parent cyclooctene.[66,67] While ROMP of low-strain cycloalkenes gives a similar recycling strategy to nonstrained lactones such as γ-butyrolactone (γ-BL)[47] wherein a polymerization−depolymerization equilibrium can be regulated by reaction temperature and monomer concentration, historically, low-strain cycloalkenes have remained largely underutilized.[68,69] Nonetheless, poly(cyclic olefin)s derived from cyclopentene derivatives[70−75] and a five-membered cyclic enol ether (2,3-dihydrofuran)[76] are recyclable through ring-closing metathesis to re-form their low-strain starting monomers. Among the low-strain cycloalkenes, cyclohexene has essentially no ring strain and thus hardly undergoes ROMP due to a lack of thermodynamic driving force,[77−80] analogous to the ROP of γ-BL. While several alternative strategies have been developed, such as ring-opening metathesis copolymerization of low to moderately strained cycloalkenes with highly strained monomers[81−87] and tandem ring-opening/ring-closing metathesis polymerization based on a selective cascade reaction between a terminal alkyne and a cyclohexene or cascade polymerization of bicycloalkene monomers,[88−92] the ROMP of cyclohexene still remains a challenge, and its potential as a circular poly(cyclic olefin) strategy to deliver high-performance materials with complete chemical recyclability has not been realized.

In our continued efforts toward developing chemically recyclable polymers,[36,47,48,50,56] we recently conceived a novel hybrid monomer design strategy that synergistically couples a high-ceiling temperature (HCT) substructure (such as ε-caprolactone) for high polymerizability/performance properties with a low-ceiling-temperature (LCT) substructure (such as γ-BL) for high depolymerizability/recyclability within the same monomer structure.[50] The offspring bicyclic lactone (BiL) can be readily polymerized under ambient conditions to high-molecular-weight poly(BiL) (PBiL) materials that exhibit both high-performance properties and complete chemical recyclability at 120 °C in the presence of a catalyst. In this work, we designed a bicyclic lactone/olefin bifunctional monomer (BiL$^{=}$) comprising "nonpolymerizable", LCT substructures of γ-BL toward ROP and cyclohexene toward ROMP, which could potentially not only be polymerizable but also render orthogonal mechanistic pathways (i.e., ROP vs ROMP, Scheme 1). Excitingly, the new hybrid monomer BiL$^{=}$ can undergo *orthogonal polymerization* between ROP and ROMP. In other words, we can produce two totally different classes of polymeric materials from one single olefin/lactone monomer BiL$^{=}$: polyester P(BiL$^{=}$)$_{ROP}$ via ROP and functionalized poly(cyclic olefin) P(BiL$^{=}$)$_{ROMP}$ via ROMP (Scheme 1). Importantly, both P(BiL$^{=}$)$_{ROP}$ and P(BiL$^{=}$)$_{ROMP}$ are chemically recyclable under mild conditions (25−40 °C). Furthermore, the intact functional group during orthogonal polymerization (i.e., the double bond in ROP and the lactone in ROMP) offers opportunity to further functionalize these two resulting polymers for tuning performance property variations. Several systems were reported wherein one monomer could undergo two different polymerization pathways to afford two different polymers[41] or one identical polymer;[93] however, those systems had to compromise between several trade-offs and did not achieve chemical recyclability for both polymers.

RESULTS AND DISCUSSION

There are four design elements in the olefin/lactone bifunctional monomer BiL$^{=}$ (6-oxabicyclo[3.2.1]oct-3-en-7-

https://doi.org/10.1021/jacs.1c12278
J. Am. Chem. Soc. 2022, 144, 2264−2275

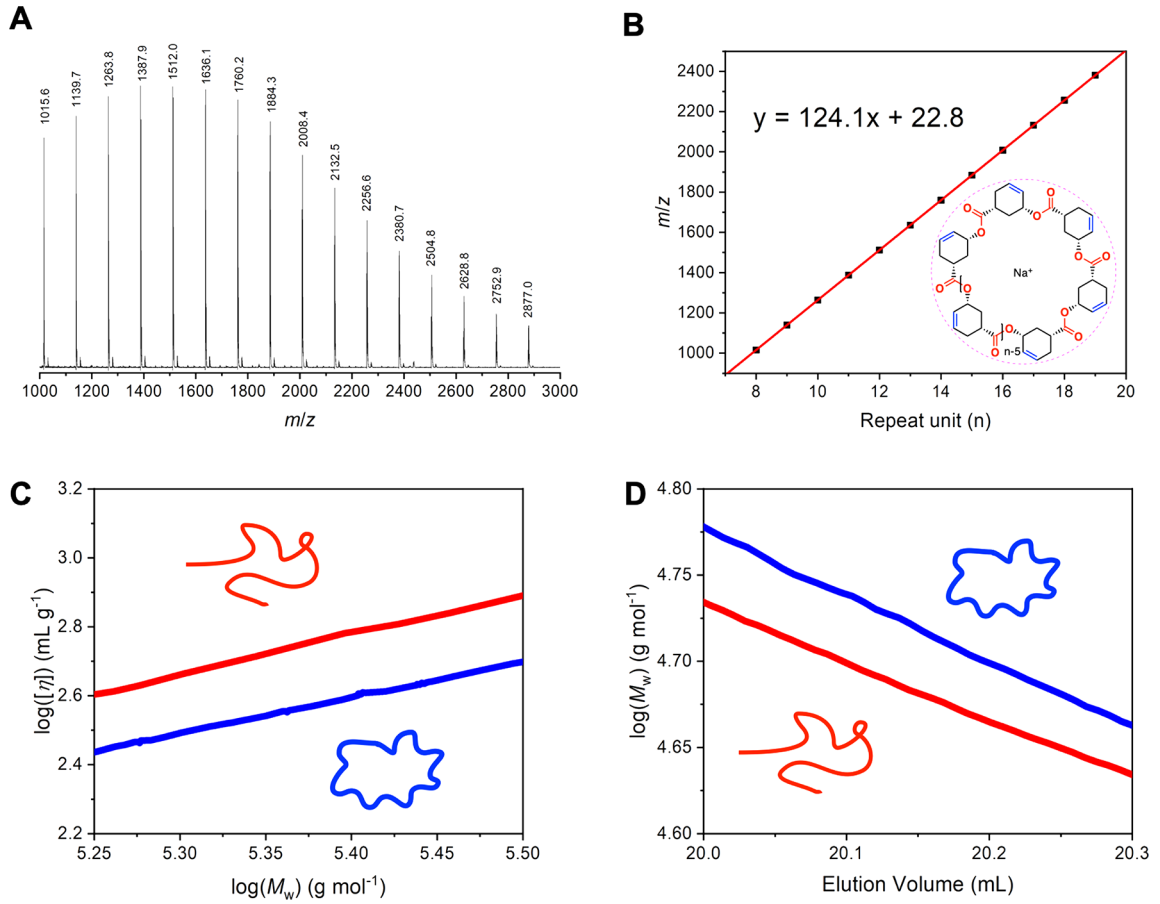

Figure 1. (A) MALDI-TOF MS spectrum of the cyclic P(BiL$^{=}$)$_{ROP}$ produced with [BiL$^{=}$]/[La-**1**] = 100/1. (B) Plot of m/z values (y) of the cyclic P(BiL$^{=}$)$_{ROP}$ versus the theoretical number of BiL$^{=}$ repeat units (x). (C) Double-logarithmic (Mark−Houwink−Sakurada) plots of intrinsic viscosity [η] vs M_w of linear (red) and cyclic (black) P(BiL$^{=}$)$_{ROP}$ produced by La-**1**/ROH and La-**1**, respectively. (D) Logarithm plots of M_w vs elution volume of linear (red) and cyclic (black) P(BiL$^{=}$)$_{ROP}$ produced by La-**1**/ROH and La-**1**, respectively.

one), reflected on by the four unique built-in substructural units (Scheme 1): in the ROP manifold, it has both the seven-membered lactone for high polymerizability and the five-membered lactone for high depolymerizability, while in the ROMP manifold, it has the appropriately strained cyclohexene for balanced (de)polymerizability due to the bridging ester moiety in the monomer and in-chain five-membered lactone ring in the polymer. We hypothesized that by this design the hybrid BiL$^{=}$ monomer would exhibit orthogonal ROP and ROMP (de)polymerizability although both parents γ-BL and cyclohexene are notoriously "nonpolymerizable" or only polymerizable under harsh conditions in the corresponding ROP and ROMP method. The hybrid BiL$^{=}$ can be synthesized from 3-cyclohexene-1-carboxylic acid via a scalable (60 g), two-step reaction with a high overall isolated yield ~94%. Worth noting here is that the carboxylic acid is readily obtainable from acrylic acid and 1,3-butadiene via the quantitative Diels−Alder reaction.

ROP Manifold. Both the widely practiced, commercially available organic catalyst 1,5,7-triazabicyclo[4.4.0]dec-5-ene (TBD) and metal-based catalyst La[N(SiMe$_3$)$_2$]$_3$ (La-**1**) were employed for initial screening of polymerization conditions. Specially, the TBD-catalyzed ROP in toluene (6.0 M) at room temperature (RT, ~25 °C) with [BiL$^{=}$]/[TBD]/[BnOH] = 100/1/1 (BnOH = benzyl alcohol, as the initiator) achieved 98% conversion after 12 h, affording P(BiL$^{=}$)$_{ROP}$ with a low number-average molecular weight (M_n) of 8.8 kg mol^{-1} and a relatively broad dispersity ($Đ$) of 1.41 (Table S1, run 1). Further exploring the ROP with [BiL$^{=}$]/[TBD]/[BnOH] = 500/1/1 in toluene (6.0 M) at RT, the monomer conversion reached to 69% after 48 h, affording P(BiL$^{=}$)$_{ROP}$ with M_n = 31.3 kg mol^{-1} and $Đ$ = 1.33 (Table S1, run 2). The resulting unsaturated polyester P(BiL$^{=}$)$_{ROP}$ is an amorphous material, with a relatively high T_g of 103 °C as a polyester. Switching to metal-catalyzed coordinative-insertion ROP, the La-**1** catalyzed polymerization achieved 89% conversion after 8 h with [BiL$^{=}$]/[La-**1**]/[BnOH] = 300/1/3 (RT, 6.0 M in toluene) (Table S1, run 3).

Surprisingly, ^{1}H NMR of the P(BiL$^{=}$)$_{ROP}$ produced by TBD revealed epimerization at the stereogenic carbon adjacent to the carbonyl carbon which took place during the ROP, thus affording the P(BiL$^{=}$)$_{ROP}$ containing both *cis* (69%) and *trans* (36%) stereoconfigurations (Figure S3A). The ^{1}H NMR spectrum exhibited two sets of peaks at both the alkoxy methine proton [−C*H*O−] region (labels c and c′ for *cis*- and *trans*- configurations, respectively) and the [−C*H*═C*H*−] methine proton regions (labels a,b and a′,b′ for *cis*- and *trans*-configurations, respectively). In contrast, the P(BiL$^{=}$)$_{ROP}$ produced by the metal-catalyzed coordinative-insertion ROP completely retains the *cis*-configuration without noticeable epimerization, based on ^{1}H NMR analysis (Figure S3A vs Figure S3B). Specifically, the ^{1}H NMR spectrum of the P(BiL$^{=}$)$_{ROP}$ produced by La-**1** displayed no peaks associated with the *trans*-configuration (i.e., a′, b′, and c′ labeled peaks

https://doi.org/10.1021/jacs.1c12278
J. Am. Chem. Soc. 2022, 144, 2264−2275

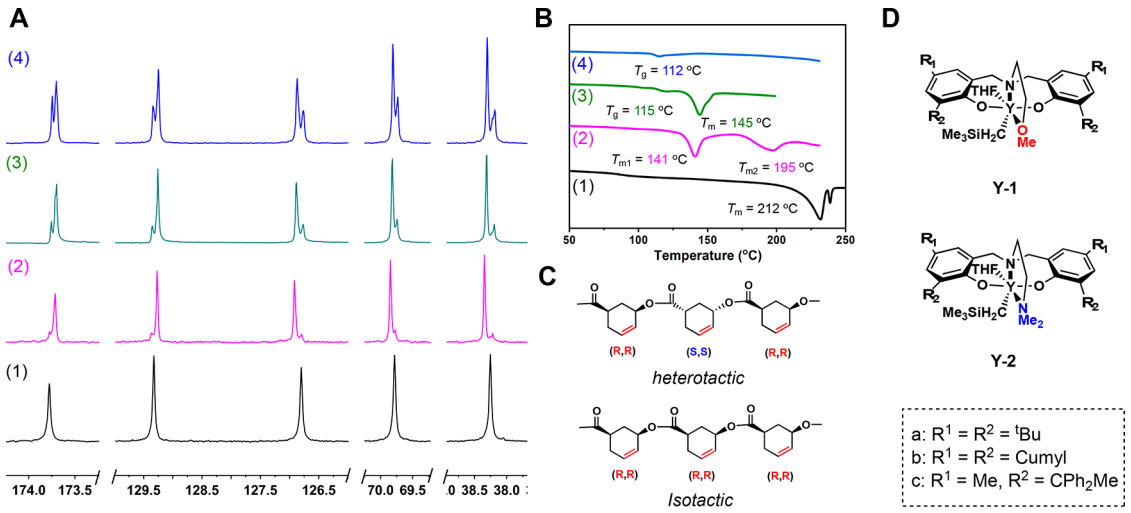

Figure 2. (A) ^{13}C NMR spectra of P(BiL$^{=}$)$_{ROP}$ with varied stereoregularities. (B) DSC curves of first-heating scans at 10 °C/min, except (1) from the second-heating scan. (C) Structures of heterotactic and isotactic P(BiL$^{=}$)$_{ROP}$. (D) Chemical structures of the catalysts. P(BiL$^{=}$)$_{ROP}$ sample codes: (1) isotactic P(BiL$^{=}$)$_{ROP}$ from (*S*,*S*)-BiL$^{=}$ (P_m = 1.00); (2) heterotactic P(BiL$^{=}$)$_{ROP}$ from the ROP of *rac*-BiL$^{=}$ catalyzed by Y-**2**(c) (P_r = 0.93); (3) heterotactic-enriched P(BiL$^{=}$)$_{ROP}$ from the ROP of *rac*-BiL$^{=}$ catalyzed by Y-**2**(b) (P_r = 0.78); (4) amorphous P(BiL$^{=}$)$_{ROP}$ prepared by Y-**2**(a) (P_r = 0.57).

attributed to epimerization, Figure S3A). Additionally, the resulting polymer obtained by La-**1** had a narrow $Đ$ of 1.17 as compared to the considerably higher $Đ$ value of 1.41 for the TBD-derived P(BiL$^{=}$)$_{ROP}$. These results are consistent with literature reports that strongly basic TBD often causes side reactions during polymerization, such as transesterification and epimerization.[94−96]

Controlling the Topology of P(BiL$^{=}$)$_{ROP}$. On the basis of our prior observations that La-**1**, when used alone (i.e., in the absence of an alcohol co-initiator), produces cyclic polyesters in the ROP of lactones,[47,48,50] we investigated the ROP of BiL$^{=}$ by La-**1** alone, aiming to produce cyclic P(BiL$^{=}$)$_{ROP}$. With a [BiL$^{=}$]/[La-**1**] ratio of 100/1 in toluene, 60% conversion was achieved at RT after 8 h (Table S1, run 4), affording P(BiL$^{=}$)$_{ROP}$ with M_n = 20.1 kg mol^{-1} and $Đ$ = 1.74. The targeted cyclic topology was confirmed by matrix-assisted laser desorption/ionization time-of-flight mass spectrometry (MALDI-TOF MS) and gel-permeation chromatography (GPC) with light scattering, refractive index, and viscosity triple detection in chloroform (Figure 1). Specifically, the MS of the P(BiL$^{=}$)$_{ROP}$ produced by La-**1** without the BnOH initiation consisted of only one series of molecular ion peaks, with the identical spacings between the two neighboring molecular ion peaks being that of the exact molar mass of the repeat unit (m/z = 124.1), as shown by the slope (124.0) of the linear plot of m/z values (y) vs the number of BiL$^{=}$ repeat units (x). The intercept of 22.8 accounts for the mass of Na^+, revealing no end groups for the cyclic P(BiL$^{=}$)$_{ROP}$ structure (Figure 1A,B). To provide further experimental evidence to distinguish between the linear and cyclic P(BiL$^{=}$)$_{ROP}$ topologies, a Mark−Houwink plot (i.e., double-logarithmic plots of intrinsic viscosity [η] vs absolute weight-average molecular weight (M_w) determined by light scattering detection) of the linear P(BiL$^{=}$)$_{ROP}$ and the cyclic P(BiL$^{=}$)$_{ROP}$ is presented in Figure 1C. As expected, the cyclic P(BiL$^{=}$)$_{ROP}$ exhibited a lower intrinsic viscosity than its linear analogue, consistent with the theoretically predicted value for cyclic polymers. When the M_w's of these linear and cyclic analogues are compared per elution volume as functions of hydrodynamic radius, the cyclic P(BiL$^{=}$)$_{ROP}$ has higher M_w than its linear analogue, which revealed the cyclic P(BiL$^{=}$)$_{ROP}$ has a smaller hydrodynamic volume (Figure 1D).

Controlling the Stereomicrostructure of P(BiL$^{=}$)$_{ROP}$. The stereoretention afforded by La-catalyzed ROP provides the opportunity to produce *perfectly isotactic* P(BiL$^{=}$)$_{ROP}$ starting from chiral monomer (1*S*,5*S*)-6-oxabicyclo[3.2.1]-octan-7-one [(*S*,*S*)-BiL$^{=}$], synthesized from commercial reagent (*S*)-(−)-3-cyclohexenecarboxylic acid. The ROP with [(*S*,*S*)-BiL$^{=}$]/[La-**1**]/[BnOH] = 600/1/3 yielded the corresponding chiral polymer P[(*S*,*S*)-BiL$^{=}$]$_{ROP}$ with M_n = 17.3 kg mol^{-1} and $Đ$ = 1.18 at 86% conversion. As anticipated, the resulting polymer is purely isotactic, displaying no observable stereoerrors on its ^{13}C NMR (P_m = 1.00, Figure S13). This chiral polymer exhibited a very high T_m of 239 °C on the differentiation scanning calorimetry (DSC) second heating scan with a crystallization temperature of 212 °C (Figure S14). When *rac*-BiL$^{=}$ was polymerized by achiral catalyst La-**1**, only iso-enriched P(BiL$^{=}$)$_{ROP}$ was produced with a low tacticity of P_r = 0.35 (Figure S9). The fact that the stereocenters contained in the monomer are in a *cis*-configuration, which remains unperturbed by the metal-catalyzed ROP, implies that isotactic (*R*,*R*−*R*,*R* and *S*,*S*−*S*,*S*) and heterotactic (*R*,*R*−*S*,*S*) sequences are the only possible products from the *rac*-BiL$^{=}$ ROP because the syndiotactic sequence (*R*,*S*−*R*,*S*) is only obtainable by epimerization. Thus, to improve the stereoselectivity of the ROP of *rac*-BiL$^{=}$, we next employed discrete yttrium silylamido {N(SiHMe$_2$)$_2$} complexes supported by C_2-symmetric *N*,*N*′-bis(salicylidene)cyclohexanediimine (salcy) ligands since such catalysts have been shown to mediate site-controlled highly isoselective polymerization of eight-membered *rac*-diolides by enantiomorphic-site control.[97,98] However, the use of [Y]{N(SiHMe$_2$)$_2$} complexes supported by 3,5-CMe$_3$-substituted salcy and 3-CPh$_3$-5-Me-substituted salcy ligands only afforded an amorphous material with low tacticity (P_r = 0.35−0.45) (Table S1, runs 5−7, and Figures S16−S18).

Subsequently, more sterically encumbered discrete yttrium alkyl complexes supported by tetradentate amino-bisphenolate ligands[99,49] with β-OMe (Y-**1**) or β-NMe$_2$ (Y-**2**) side-arm

https://doi.org/10.1021/jacs.1c12278
J. Am. Chem. Soc. 2022, 144, 2264−2275

donor (Figure 2D) were employed for the ROP of *rac*-BiL$^{=}$ to induce chain-end controlled heteroselectivity. At the outset, *tert*-butyl-substituted complex Y-**1**(a) in toluene also afforded an atactic polymer (P_r = 0.35) (Table S2, run 1). Tuning the reaction conditions by using dichloromethane (DCM) instead of toluene further enhanced the P_r value to 0.49 (Table S2, run 2), which was assessed by ^{13}C NMR spectra (Figures S19 and S20). Further increasing the steric hindrance of the bisphenolate ligand to ortho-cumyl [Y-**1**(b)] in toluene and DCM still afforded atactic polymers but with increased P_r value to 0.59 and 0.74 (Table S2, runs 3 and 4; Figures S21 and S22), respectively, which indicated that DCM is more effective for producing high heterotacticity. We also conducted the ROP without solvent, which gave a P_r value of 0.66 (Table S2, run 5, and Figure S23), midway between toluene (P_r = 0.59) and DCM (P_r = 0.74). Thus, the solvent has a significant impact on the chain end selectivity of *rac*-BiL$^{=}$. ROP of *rac*-BiL$^{=}$ at −30 °C in toluene by Y-**1**(b) gave a decreased P_r of 0.45 (Table S2, run 6, and Figure S24).

Manipulating the catalyst ligand side arm (the pendant donor group) has been shown to be an effective strategy for the design of organometallic catalysts for asymmetric organic reactions.[49,100] Indeed, changing the side-arm donor from β-OMe in Y-**1**(b) to β-NMe_2 generated Y-**2**(b) which drastically increased selectivity and produced heterotactic-enriched P-(BiL$^{=}$)$_{ROP}$ (P_r = 0.71 in toluene or P_r = 0.78 in DCM; Table S2, runs 9 and 10; Figures S27 and S28). Excitingly, with the increased heterotacticity, the P(BiL$^{=}$)$_{ROP}$ material derived from Y-**2**(b) in DCM finally became semicrystalline, as evidenced by their endothermic first-order melting transition with a high T_m value of 145 °C as shown in Figure 2B.

With the above informative observations, we envisioned that complex Y-**2**(c) with even bulkier −$CMePh_2$ substituents would be more selective to realize highly heteroselective ROP, Indeed, when the ROP of *rac*-BiL$^{=}$ was catalyzed by Y-**2**(c) at [*rac*-BiL$^{=}$]/[Y] ratio of 100/1, 90% conversion was achieved after 12 h, affording semicrystalline P(BiL$^{=}$)$_{ROP}$ with M_n = 16.0 kg mol^{-1}, $Đ$ = 1.09, and P_r = 0.93 (Table S2, run 11, and Figure S29). The heterotactic microstructure of the resulting P(BiL$^{=}$)$_{ROP}$ can be confirmed by comparing with the purely isotactic microstructure obtained from the stereoretention ROP of enantiopure monomer (*S*,*S*)-BiL$^{=}$ (Figures 2A(1) and 2C). Intriguingly, the heterotactic-enriched P(BiL$^{=}$)$_{ROP}$ exhibited two melting temperatures (T_{m1} = 141 °C, T_{m2} = 195 °C) on the DSC first heating scan (Figure 2B). When precatalyst Y-**2**(c) was combined with 1 equiv of BnOH initiator for a more controlled polymerization, the heterotacticity of the resulting P(BiL$^{=}$)$_{ROP}$ decreased slightly to 0.91 (Table S2, run 12, and Figure S30). However, the BnOH initiation system is well-controlled and follows strictly first-order kinetics (R^2 = 0.998) up to high conversions with molecular weight increasing linearly with monomer conversion while maintaining low dispersity ($Đ$ < 1.1) (Figure S32).

ROMP Manifold. After realizing the topologically controlled and stereoselective ROP of BiL$^{=}$, we subsequently turned our attention to the ROMP pathway of BiL$^{=}$. In contrast to the ROP product P(BiL$^{=}$)$_{ROP}$, which is a polyester with cyclohexene incorporated in the repeating unit, the ROMP product P(BiL$^{=}$)$_{ROMP}$ is a poly(cyclic olefin) with C−C and C═C bonds in the main-chain backbone (Scheme 1).

Several Grubbs catalysts were screened for the ROMP of BiL$^{=}$. When ROMP of BiL$^{=}$ was performed with the Grubbs third-generation catalyst (G3) (Table S3), the polymerization proceeded rapidly at RT with varied monomer concentrations (1.9 to 5.0 M) and [BiL$^{=}$]/[G3] feed ratios (1000/1 to 40000/1). However, the measured M_n values of the resulting poly(cyclic olefin)s deviated significantly from the theoretical values. Next, the Grubbs second-generation catalyst (G2) was used (Table S4), which afforded high-molecular-weight P(BiL$^{=}$)$_{ROMP}$ (M_n up to 340.2 kg mol^{-1}, $Đ$ ∼ 1.3). Specifically, the ROMP of BiL$^{=}$ performed in DCM (5.0 M) at RT with [BiL$^{=}$]/[G2] = 10000/1 gelled after 1 h and achieved 80% monomer conversion after 24 h. The resulting P(BiL$^{=}$)$_{ROMP}$ had a higher M_n of 58.7 kg mol^{-1} than the P(BiL$^{=}$)$_{ROMP}$ produced from G3, and the dispersity was relatively narrow ($Đ$ = 1.23) (Table S4, run 1). Increasing the [BiL$^{=}$]/[G2] ratio to 20000/1 gave a higher M_n (89.6 kg mol^{-1}, $Đ$ = 1.29), while the monomer conversion decreased to 51% (Table S4, run 2). Further lowering the catalyst loading to 25 ppm ([BiL$^{=}$]/[G2] = 40000/1), the monomer conversion reached only 45% after 24 h, affording a higher molecular weight P(BiL$^{=}$)$_{ROMP}$ with M_n = 96.6 kg mol^{-1} and $Đ$ = 1.26 (Table S4, run 3). These results indicated that the G2 catalyst exhibited better control for the ROMP of BiL$^{=}$, and the catalyst loading can be as low as 25 ppm. Heterogeneous polymerizations of BiL$^{=}$ were performed in toluene and solvent free conditions to yield higher molecular weight P(BiL$^{=}$)$_{ROMP}$ with M_n up to 340 kg mol^{-1} and unimodal distribution (Table S4, Figures S37 and S38).

The ROMP of enantiopure (*S*,*S*)-BiL$^{=}$ exhibited similar polymerization behavior as *rac*-BiL$^{=}$. Specifically, the P[(*S*,*S*)-BiL$^{=}$]$_{ROMP}$ produced in DCM had a medium M_n of 23.1 kg mol^{-1} (Table S4, run 16), while ROMP of (*S*,*S*)-BiL$^{=}$ in toluene afforded a high M_n of 276 kg mol^{-1} with a relatively narrow dispersity of 1.28 (Table S4, run 17). The structural differences can be observed by comparing the ^{13}C NMR of the P(BiL$^{=}$)$_{ROMP}$ and P[(*S*,*S*)-BiL$^{=}$]$_{ROMP}$. The peak splitting of P[(*S*,*S*)-BiL$^{=}$]$_{ROMP}$ is clearer than that of P(BiL$^{=}$)$_{ROMP}$; however, the connection between two adjacent units is not regioselective, with both head-to-tail and head-to-head connections and *cis*/*trans* alkene configurations possible (Figures S34 and S36). As a result, the P[(*S*,*S*)-BiL$^{=}$]$_{ROMP}$ derived from the enantiopure monomer is an amorphous material displaying a similar T_g of 111 °C to that of the P(BiL$^{=}$)$_{ROMP}$ (Figures S39 and S40).

Chemical Recyclability of P(BiL$^{=}$)$_{ROMP}$ and P(BiL$^{=}$)$_{ROP}$. To quantify the polymerizability of BiL$^{=}$ and depolymerizability of P(BiL$^{=}$)$_{ROMP}$ as a function of reaction conditions, the ROMP thermodynamics of the BiL$^{=}$ polymerization was probed by using [BiL$^{=}$]/[G3] = 100/1 and [BiL$^{=}$]$_0$ = 0.5 mol L^{-1} in CD_2Cl_2 via a variable-temperature NMR study. The equilibrium monomer concentration, [BiL$^{=}$]$_{eq(ROMP)}$, obtained by plotting [BiL$^{=}$]$_t$ as a function of time until [BiL$^{=}$] became constant, was measured to be 0.380, 0.285, 0.245, and 0.215 mol L^{-1} for 25, 15, 10, and 5 °C, respectively. The van't Hoff plot of ln[BiL$^{=}$]$_{eq}$ vs $1/T$ gave a straight line (R^2 = 0.998, Figures S41 and S42), from which the thermodynamic parameters were calculated to be ΔH_p^o = −19.8 kJ mol^{-1} and ΔS_p^o = −58.3 J mol^{-1} K^{-1}, based on the equation $\ln[\text{BiL}^{=}]_{eq} = \Delta H_p^o/RT - \Delta S_p^o/R$. The T_c value was calculated to be 506 K (233 °C) in bulk or 340 K (66.4 °C) at [BiL$^{=}$]$_0$ = 1.0 mol L^{-1}, based on the equation $T_c = \Delta H_p^o/\{\Delta S_p^o + R \ln[\text{BiL}^{=}]_0\}$. Similarly, the ROP thermodynamics of the BiL$^{=}$ polymerization was also probed via variable-temperature ^{1}H NMR at the conditions of [BiL$^{=}$]/[La-**1**]/[BnOH] = 100/1/3 and [BiL$^{=}$]$_0$ = 0.5 mol L^{-1} in toluene-d_8. The [BiL$^{=}$]$_{eq(ROP)}$ was measured to be 0.155, 0.130, 0.105, and 0.070 mol L^{-1} for 60,

https://doi.org/10.1021/jacs.1c12278
J. Am. Chem. Soc. 2022, 144, 2264−2275

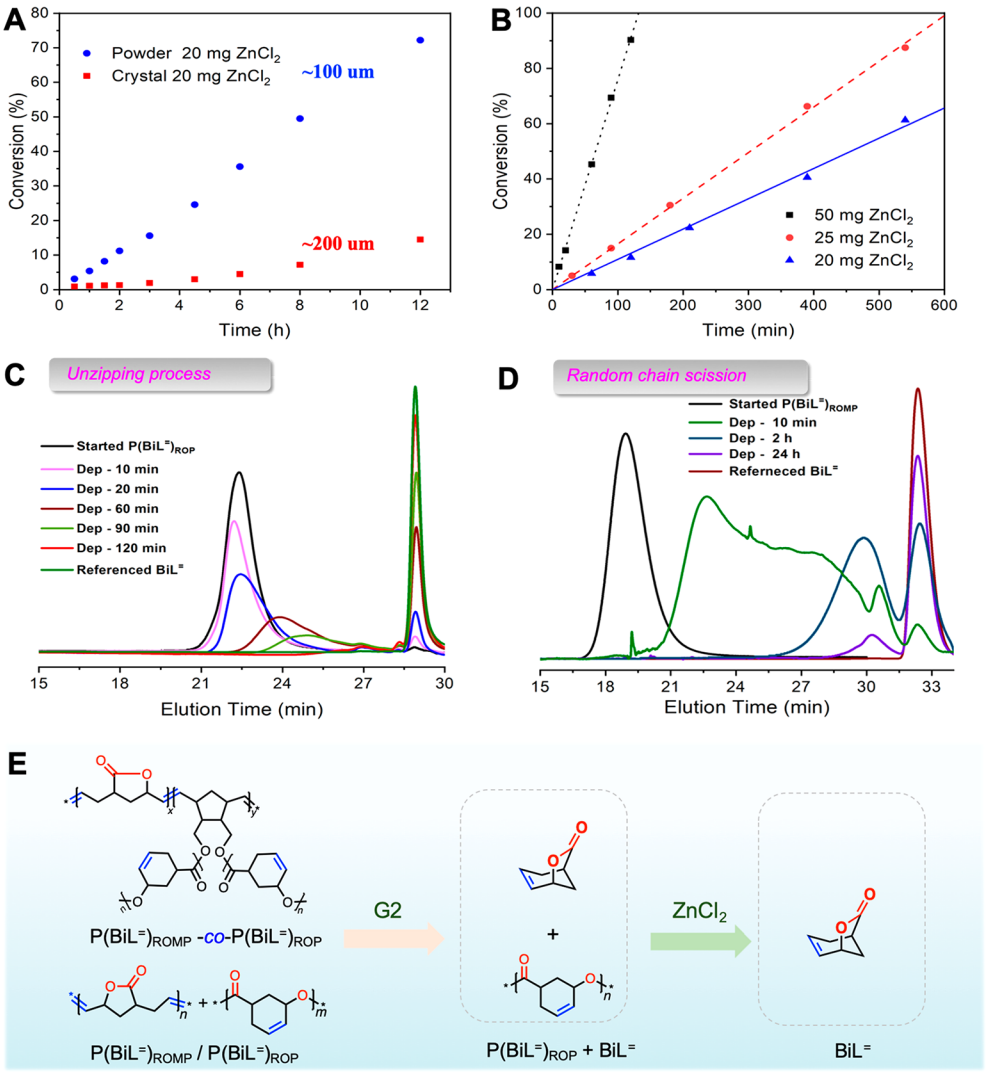

Figure 3. (A) $P(BiL^{=})_{ROP}$ depolymerization time−conversion kinetics data as a function of $ZnCl_2$ particle size. (B) $P(BiL^{=})_{ROP}$ depolymerization kinetics data as a function of $ZnCl_2$ loading. (C) Monitoring of $P(BiL^{=})_{ROP}$ depolymerization by GPC in $CHCl_3$. (D) Monitoring of $P(BiL^{=})_{ROMP}$ depolymerization by GPC in DCM. (E) Schematic illustration of orthogonal depolymerization of copolymer $P(BiL^{=})_{ROMP}$-*co*-$P(BiL^{=})_{ROP}$ and physical blend $P(BiL^{=})_{ROMP}$/$P(BiL^{=})_{ROP}$.

55, 50, and 40 °C, respectively. Subsequently, the ROP thermodynamic parameters were obtained to be $\Delta H_p^o = -34.7$ kJ mol^{-1} and $\Delta S_p^o = -88.7$ J mol^{-1} K^{-1}, and the T_c value was calculated to be 391 K (118 °C) at $[BiL^{=}]_0 = 1.0$ mol L^{-1} (Figures S43 and S44). These results indicate both good polymerizability of $BiL^{=}$ and medium depolymerizability of the functionalized poly(cyclic olefin) $P(BiL^{=})_{ROMP}$ and polyester $P(BiL^{=})_{ROP}$.

Indeed, the ROMP and ROP results summarized in Table S1−S4 are consistent with the above-derived thermodynamic parameters. Next, we examined the depolymerizability of $P(BiL^{=})_{ROMP}$ and $P(BiL^{=})_{ROP}$. We first probed the depolymerizability of the preformed $P(BiL^{=})_{ROMP}$ ($M_n = 96.6$ kg mol^{-1}, $Đ = 1.26$) using G2 at RT under dilute conditions (10 mg/mL), which is limited by the solubility of $P(BiL^{=})_{ROMP}$. The depolymerization of $P(BiL^{=})_{ROMP}$ in CD_2Cl_2 was monitored *in situ* by ^{1}H NMR, revealing that the depolymerization was almost complete after 24 h to cleanly regenerate the monomer $BiL^{=}$ (Figure S45). This depolymerization was also monitored *in situ* by GPC; after stirring with 0.2 mol % G2 catalyst at RT for 10 min, the trace of the initial unimodal $P(BiL^{=})_{ROMP}$ turned into a broad peak with lower molecular weight fractions appearing, at which point only 2% $BiL^{=}$ was regenerated (by ^{1}H NMR integration), indicating a *random chain scission process* in the depolymerization of $P(BiL^{=})_{ROMP}$ catalyzed by G2. After 24 h, the $P(BiL^{=})_{ROMP}$ was nearly completely depolymerized with the disappearance of the polymer peak and increase of the monomer peak (Figure 3D). Increasing the depolymerization temperature and catalyst loading significantly shortened the depolymerization time (Figure S46). In addition, we also conducted the $P(BiL^{=})_{ROMP}$ depolymerization on the 28 g scale, wherein the depolymerization was performed with 0.1 mol % G2 catalyst in DCM; after refluxing for 24 h in open air, the catalyst was removed by flash column chromatography, and the pure $BiL^{=}$ monomer was recovered in 93% yield. These results demonstrate the excellent recyclability of $P(BiL^{=})_{ROMP}$.

With the success of chemical recycling $P(BiL^{=})_{ROMP}$ under mild conditions, we then set out to determine whether the resulting polyester $P(BiL^{=})_{ROP}$ could also be recycled. Comparing to its saturated analogue, the T_c value (118 °C) of $P(BiL^{=})_{ROP}$ at $[BiL^{=}]_0 = 1.0$ mol L^{-1} is about 12 °C higher than the saturated monomer BiL ($\Delta H_p^o = -21.1$ kJ mol^{-1}, ΔS_p^o

https://doi.org/10.1021/jacs.1c12278
J. Am. Chem. Soc. 2022, 144, 2264−2275

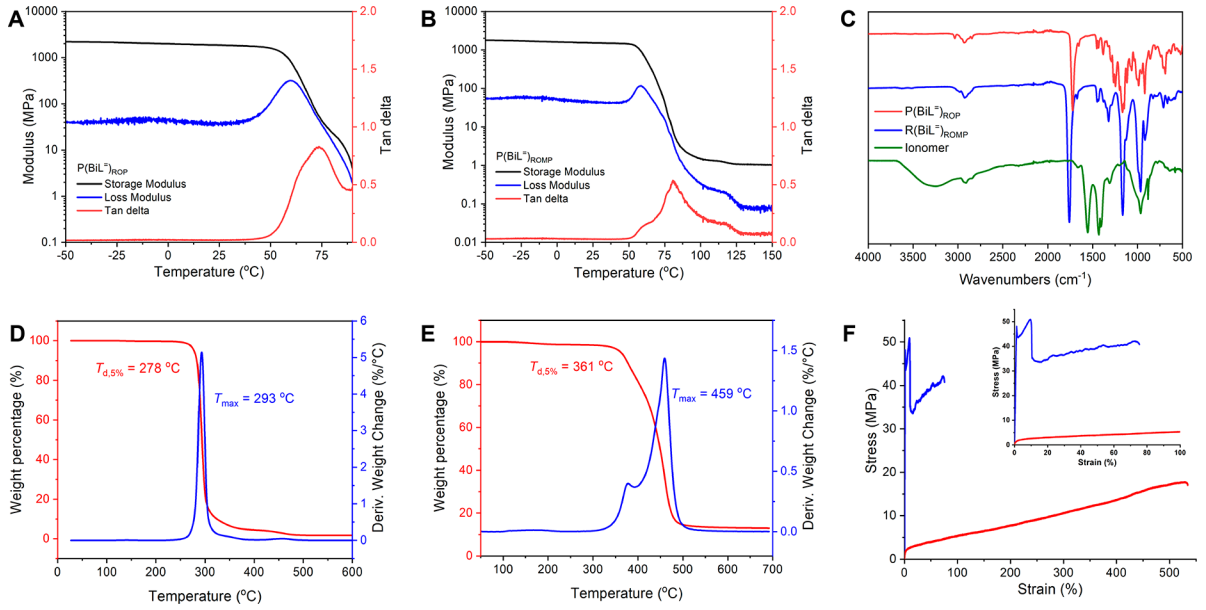

Figure 4. (A) Overlay of storage modulus E', loss modulus E'', and tan δ for $P(BiL^{=})_{ROP}$ (M_n = 31.3 kg mol^{-1}) by DMA (tension film mode, 0.05% strain, 1 Hz, 3 °C min^{-1}). (B) Overlay of E', E'', and tan δ for $P(BiL^{=})_{ROMP}$ (M_n = 334.2 kg mol^{-1}) by DMA (tension film mode, 0.05% strain, 1 Hz, 3 °C min^{-1}). (C) Overlays of FT-IR spectra for $P(BiL^{=})_{ROP}$, $P(BiL^{=})_{ROMP}$, and the ionomer. (D) TGA and DTG (at 10 °C min^{-1} heating rate) thermograms of $P(BiL^{=})_{ROP}$ produced by TBD (M_n = 31.3 kg mol^{-1}). (E) TGA and DTG curves for $P(BiL^{=})_{ROMP}$ (M_n = 89.6 kg mol^{-1}). (F) Stress−strain curves for the $P(BiL^{=})_{ROMP}$ prepared by G2 (M_n = 333 kg mol^{-1}, blue curve) and the ionomer prepared by hydrolysis of $P(BiL^{=})_{ROMP}$ (red curve). Inset: blowup region from 0 to 100% elongation.

= −55.8 J mol^{-1} K^{-1}, T_c = 106 °C), which corresponds to the higher ring strain due to the introduction of the C=C double bond in the monomer structure.[50] Thus, we first tried the exactly the same conditions as those employed for the depolymerization of the saturated analogue. However, the depolymerization of $P(BiL^{=})_{ROP}$ actually proved to be difficult, as $P(BiL^{=})_{ROP}$ contains a reactive site C=C bond that induces side reactions during the high-temperature depolymerization conditions.

Subsequently, we explored the depolymerization of $P(BiL^{=})_{ROP}$ catalyzed by $ZnCl_2$ in toluene-d_8 (10 mg/mL) at 120 °C but observed only around 20% conversion back to monomer due to side reactions that decomposed the majority (~80%) of $P(BiL^{=})_{ROP}$ after 24 h. When we turned to TBD under the same conditions, an increase in monomer recovery up to 40% after 24 h was achieved, but still the same decomposition was observed. Thus, side reactions outcompete the depolymerization at high temperatures, but such conditions are necessary for most polyesters to overcome the depolymerization energy barrier.[48,50] To suppress or avoid the temperature-induced side reactions, we turned our attention to low-temperature depolymerization aided by a Lewis acidic catalyst. Excitingly, depolymerization of $P(BiL^{=})_{ROP}$ with $ZnCl_2$ (~50 mg) in DCM at 40 °C regenerated 94% monomer after 12 h (Figure S47). Even an epimerized mixture of *cis*- and *trans*-$P(BiL^{=})_{ROP}$ materials produced from TBD was completely depolymerized with slightly lower selectivity (~87%, Figure S48). Fascinatingly, using the exact same condition to depolymerize the saturated analogue (PBiL) without the double bond, which has an even lower T_c value,[50] we observed no depolymerization after 24 h.

To gain further insight into the mechanism of $ZnCl_2$-catalyzed depolymerization of $P(BiL^{=})_{ROP}$, we ascertained two working hypotheses. First, $ZnCl_2$ might actually react with $P(BiL^{=})_{ROP}$ to form a specific active depolymerization complex. Alternatively, simple interactions between $ZnCl_2$ and $P(BiL^{=})_{ROP}$ alkene/carbonyl might augment the conformation of the $P(BiL^{=})_{ROP}$ so that the energy barrier for ring-closing depolymerization is lowered. To this end, we employed $ZnCl_2$ to depolymerize a mixture of $P(BiL^{=})_{ROP}$ and PBiL under the same conditions. If a specific zinc complex formed, it should also be active for the depolymerization of lower ring-strain analogue PBiL. However, only $P(BiL^{=})_{ROP}$ was selectively depolymerized while PBiL was left untouched (Figure S49), which indicates the hypothesis of an active catalyst formed *in situ* is less probable. Furthermore, additional zinc compounds were tested, such as zinc acetate, zinc acetylacetonate, and [(β-diketiminate)Zn(TMS)$_2$], but none of these compounds catalyzed the depolymerization of $P(BiL^{=})_{ROP}$. Subsequently, we explored the $ZnCl_2$ particle size effect on $P(BiL^{=})_{ROP}$ depolymerization, with the as-received crystalline $ZnCl_2$ having a diameter of ~200 μm, as estimated by scanning electron microscopy (SEM), and the grinded powder $ZnCl_2$ of ~100 μm (Figure S50). Depolymerization kinetics with the same amount (20 mg) of crystalline and powdery $ZnCl_2$ were conducted. The powdery $ZnCl_2$ showed higher activity, achieving 72% monomer recovery in 12 h, while the crystalline $ZnCl_2$ only afforded 15% monomer recovery in 12 h (Figure 3A). These results indicated the higher the surface area of $ZnCl_2$, the higher the depolymerization rate is. As additional corroborative evidence, the $ZnCl_2$ loading also showed a significant effect on $P(BiL^{=})_{ROP}$ depolymerization: the depolymerization rate increased with the increasing of the powdery $ZnCl_2$ loading, and the kinetics data showed the monomer recovery yield was increased linearly with the time (Figure 3B). These results indicated the depolymerization follows zero-order kinetics and is consistent with the interfacial catalytic mechanism. Furthermore, in contrast to the depolymerization of $P(BiL^{=})_{ROMP}$, *in situ* monitoring of the depolymerization of $P(BiL^{=})_{ROP}$ (M_n = 24.7 kg mol^{-1}, $Đ$ =

https://doi.org/10.1021/jacs.1c12278
J. Am. Chem. Soc. 2022, 144, 2264−2275

1.15) by GPC indicated that the depolymerization follows an unzipping mechanism rather than a random chain scission process (Figure 3C). Lastly, changing the solvent from CD_2Cl_2 to a coordinating solvent (THF), which would compete with the $P(BiL^{=})_{ROP}$ alkene and carbonyl for interaction with $ZnCl_2$, gave no depolymerization of $P(BiL^{=})_{ROP}$.

The success of achieving the monomer recovery of both $P(BiL^{=})_{ROMP}$ and $P(BiL^{=})_{ROP}$ further inspired us to pursue the orthogonality on the depolymerization of $P(BiL^{=})_{ROMP}$ and $P(BiL^{=})_{ROP}$. First, a 1/1 mixture of $P(BiL^{=})_{ROMP}$ and $P(BiL^{=})_{ROP}$ (a physical blend) was dissolved in CD_2Cl_2 with 1 wt % G2 catalyst added, and the ring-closing metathesis depolymerization of $P(BiL^{=})_{ROMP}$ went smoothly and selectively, without touching $P(BiL^{=})_{ROP}$. Then, $ZnCl_2$ was added to start the $P(BiL^{=})_{ROP}$ depolymerization once the $P(BiL^{=})_{ROMP}$ was completely depolymerized into the monomer $BiL^{=}$. The depolymerization results showed excellent orthogonality on the selective depolymerization of $P(BiL^{=})_{ROMP}$ and $P(BiL^{=})_{ROP}$, depending on the catalyst added (Figure 3E and Figure S51). The same strategy also successfully applied to the depolymerization of the copolymer of $P(BiL^{=})_{ROMP}$ and $P(BiL^{=})_{ROP}$ (Figure 3E and Figure S52).

Thermomechanical Properties of $P(BiL^{=})_{ROMP}$ and $P(BiL^{=})_{ROP}$. The differences in material properties between $P(BiL^{=})_{ROMP}$ and $P(BiL^{=})_{ROP}$ were studied next. The thermomechanical properties of $P(BiL^{=})_{ROP}$ prepared with TBD (M_n = 31.3 kg mol^{-1}, $Đ$ = 1.33) and $P(BiL^{=})_{ROMP}$ prepared with G2 (M_n = 334 kg mol^{-1}, $Đ$ = 1.31) were examined by dynamic mechanical analysis (DMA) in a tension film mode. The thermomechanical spectra of $P(BiL^{=})_{ROP}$ (Figure 4A) and $P(BiL^{=})_{ROMP}$ (Figure 4B) show that at room temperature (the glassy state) both $P(BiL^{=})_{ROP}$ and $P(BiL^{=})_{ROMP}$ exhibit high storage modulus (E') values, although E' (2.16 ± 0.29 GPa) of $P(BiL^{=})_{ROP}$ was higher than that (1.65 ± 0.13 GPa) of $P(BiL^{=})_{ROMP}$.

However, after the glass transition region [T_g ~ 74−90 °C, as defined by the peak maxima of tan δ, the loss modulus/storage modulus ratio (E''/E')] (Figure 4A,B), E' of $P(BiL^{=})_{ROP}$ dropped and then quickly went to the viscous flow state. In contrast, E' of $P(BiL^{=})_{ROMP}$ also dropped significantly after the glass transition region but did not completely lose the strength and went to the rubbery plateau, suggesting that the $P(BiL^{=})_{ROMP}$ was cross-linked during the thermomechanical testing. Mechanical properties of $P(BiL^{=})_{ROMP}$ are discussed in the following section where direct comparisons are made between the materials before and after postfunctionalization.

Thermal property differences can be found in their thermal data. $P(BiL^{=})_{ROMP}$ is an amorphous material but exhibits a high T_g of 113 °C by DSC (Figure S39), which can be ascribed to the incorporation of the five-membered γ-BL ring into the main chain. The $P(BiL^{=})_{ROP}$ also showed a high T_g between 103 and 115 °C, depending on the microstructure and molecular weight (Figure S7 and Figure 2B). Noteworthy also is the perfectly isotactic $P(BiL^{=})_{ROP}$ and heterotactic-enriched $P(BiL^{=})_{ROP}$ display high T_m values between 141 and 239 °C, depending on the tacticity. $P(BiL^{=})_{ROMP}$ displays a high decomposition temperature ($T_{d,5\%}$, defined by the temperature at 5% weight loss) of 361 °C and a high maximum rate decomposition temperature (T_{max}) of 459 °C, as measured by thermogravimetric analysis (TGA) and derivative thermogravimetric analysis (DTG) (Figure 4E). This high T_d value is consistent with the character of poly(cyclic olefin)s. In comparison, as a polyester, $P(BiL^{=})_{ROP}$ exhibits a much lower $T_{d,5\%}$ of 278 °C (Figure 4D).

Postfunctionalization of $P(BiL^{=})_{ROP}$ and $P(BiL^{=})_{ROMP}$. The built-in functionalities of $P(BiL^{=})_{ROP}$ (the C=C bond) and $P(BiL^{=})_{ROMP}$ (the lactone) allow for their respective postfunctionalization. As expected, Fourier transform infrared (FTIR) spectra of $P(BiL^{=})_{ROP}$ and $P(BiL^{=})_{ROMP}$ showed the disubstituted C=C stretching for both polymers. The νC=C for $P(BiL^{=})_{ROP}$ is at 1653 cm^{-1}, where the disubstituted C=C is in the cyclohexene form (*cis*-), while the C=C stretching frequency for $P(BiL^{=})_{ROMP}$ is 22 cm^{-1} higher at 1675 cm^{-1}, which indicates that the C=C bond in the main chain of $P(BiL^{=})_{ROMP}$ mainly adopts the *trans*-configuration. Meanwhile, the red-shift of the C=O stretching frequency (νC=O) for $P(BiL^{=})_{ROP}$ (1723 cm^{-1}) to a wavenumber of 37 cm^{-1} lower than that for $P(BiL^{=})_{ROMP}$ is also consistent with structural differences between the ester carbonyl in $P(BiL^{=})_{ROP}$ and the lactone carbonyl in $P(BiL^{=})_{ROMP}$ (1760 cm^{-1}, Figure 4C).

Through the thiol−ene click reaction, we grafted both linear and cyclic $P(BiL^{=})_{ROP}$ with 1-octadecanethiol to give the corresponding brush polyesters. This postfunctionalization made it possible for the direct observation of their respective linear and cyclic topology (Figure 5A) by high-resolution

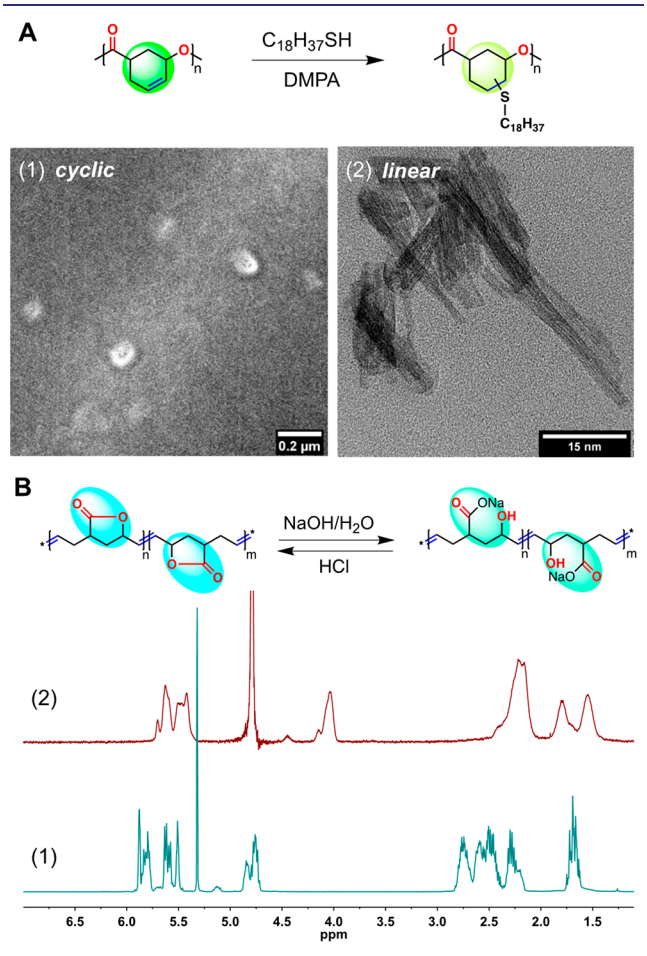

Figure 5. (A) Postfunctionalization of $P(BiL^{=})_{ROP}$ via the thiol−ene click reaction and direct observation of grafted cyclic (1) and linear (2) $P(BiL^{=})_{ROP}$ structures by TEM. (B) Reversible postfunctionalization of $P(BiL^{=})_{ROMP}$. (1) ^{1}H NMR (CD_2Cl_2) of $P(BiL^{=})_{ROMP}$ and (2) ^{1}H NMR (D_2O) of the ionomer derived from $P(BiL^{=})_{ROMP}$.

https://doi.org/10.1021/jacs.1c12278
J. Am. Chem. Soc. 2022, 144, 2264−2275

transmission electron microscopy (TEM). On the other hand, postfunctionalization of $P(BiL^{=})_{ROMP}$ utilized its built-in γ-BL ring in the main chain, which was readily hydrolyzed by NaOH to afford the carboxylate ionomer (Figure 4C, green line, and Figure 5B). This ionomer is soluble in water and stable in open air for over six months. Mechanically, $P(BiL^{=})_{ROMP}$ is best descried as a hard, strong, and tough material, as characterized by a high Young's modulus (E) of 3.8 ± 0.6 GPa, a high ultimate tensile strength (σ_B) of 40.0 ± 10.9 MPa, and a modest elongation at break (ε_B) of 76 ± 9%, attributable to the in-chain incorporated γ-BL ring. In comparison, while the ionomer produced from the hydrolysis of $P(BiL^{=})_{ROMP}$ exhibited a lower E (0.71 ± 0.15 GPa) and σ_B (18.5 ± 3.2 MPa), it is much more flexible with a high ε_B value of 445 ± 91% (Figure 4F). More excitingly, once neutralized with HCl, the carboxylate ionomer collapses back to the stable γ-BL to regenerate $P(BiL^{=})_{ROMP}$ (due to the solubility limitation, once ∼50% γ-BL was regenerated it precipitated out), demonstrating an intriguing reversible modification strategy (Figure 5B).

CONCLUSIONS

In summary, this work demonstrates the effectiveness of the monomer structural hybridization strategy to combine two LCT monomer structures, notoriously hard-to-polymerize γ-BL and cyclohexene, into an offspring lactone/olefin bifunctional monomer that renders facile polymerizability, retains depolymerizability, and yields several different classes of material options through the control of polymer structure (ROP or ROMP), topology (linear or cyclic), and microstructure (atactic, isotactic, and heterotactic tacticities). Additionally, both the resulting polymers retain built-in olefin and lactone functionalities which yield even more material possibilities through postfunctionalization.

The present hybrid monomer system also achieves the desirable but challenging orthogonality in not only the forward ROP vs ROMP process but also the backward depolymerization process, on demand simply by selecting the suitable (de)polymerization catalyst. The produced polyester $P(BiL^{=})_{ROP}$ by ROP exhibits a high T_m of 141−239 °C (from heterotactic to isotactic polymer), a high T_g of 103−115 °C, and a modest $T_{d,5\%}$ of 278 °C, while the functionalized poly(cyclic olefin) $P(BiL^{=})_{ROMP}$ by ROMP has a T_g of 113 °C and a high $T_{d,5\%}$ of 361 °C. Remarkably, despite their rather robust thermomechanical properties, both $P(BiL^{=})_{ROP}$ and $P(BiL^{=})_{ROMP}$ exhibit full chemical recyclability to regenerate the same monomer under mild conditions (25−40 °C) in the presence of a catalyst. The depolymerization orthogonality also enables selective depolymerization of both the ROP/ROMP copolymer and the physical blend composites into the same starting monomer. The comparative study with the analogous saturated polyester without the internal double bond showed the importance of designing monomer/polymer structures for achieving not only high-performance properties but also selective, low-temperature depolymerization catalysis.

Orthogonal polymerization of a bifunctional monomer offers an attractive strategy to produce two different classes of polymers from a single monomer, but a more significant, modern challenge is to additionally enable both types of the orthogonally produced polymers with orthogonal depolymerizability to recover the same monomer. This work has demonstrated that this daunting task can be achieved, thereby closing the entire one monomer−two polymers−one monomer loop.

ASSOCIATED CONTENT

Supporting Information

The Supporting Information is available free of charge at https://pubs.acs.org/doi/10.1021/jacs.1c12278.

Complete experimental details, additional figures and tables (PDF)

Accession Codes

CCDC 2122551 contains the supplementary crystallographic data for this paper. These data can be obtained free of charge via www.ccdc.cam.ac.uk/data_request/cif, or by emailing data_request@ccdc.cam.ac.uk, or by contacting The Cambridge Crystallographic Data Centre, 12 Union Road, Cambridge CB2 1EZ, UK; fax: +44 1223 336033.

AUTHOR INFORMATION

Corresponding Author

Eugene Y.-X. Chen − *Department of Chemistry, Colorado State University, Fort Collins, Colorado 80523-1872, United States*; orcid.org/0000-0001-7512-3484; Email: eugene.chen@colostate.edu

Authors

Changxia Shi − *Department of Chemistry, Colorado State University, Fort Collins, Colorado 80523-1872, United States*

Ryan W. Clarke − *Department of Chemistry, Colorado State University, Fort Collins, Colorado 80523-1872, United States*

Michael L. McGraw − *Department of Chemistry, Colorado State University, Fort Collins, Colorado 80523-1872, United States*

Complete contact information is available at: https://pubs.acs.org/10.1021/jacs.1c12278

Funding

This work by C.S. and E.Y.-X.C. was supported by the U.S. Department of Energy, Office of Energy Efficiency and Renewable Energy, Advanced Manufacturing Office (AMO) and Bioenergy Technologies Office (BETO). This work was performed as part of the BOTTLE Consortium and funded under Contract DE-AC36-08GO28308 with the National Renewable Energy Laboratory, operated by Alliance for Sustainable Energy. The work by R.W.C., M.L.M., and E.Y.-X.C. was supported by the U.S. National Science Foundation (NSF-1904962).

Notes

The authors declare no competing financial interest.

ACKNOWLEDGMENTS

We gratefully acknowledge Prof. Haixin Lin for the helpful discussions and Dr. Roy Geiss for his help acquiring TEM images.

REFERENCES

(1) Report of the Basic Energy Sciences Roundtable on Chemical Upcycling of Polymers. https://science.osti.gov/-/media/bes/pdf/reports/2020/Chemical_Upcycling_Polymers.pdf (April 30−May 1, 2019, released in February 2020, and accessed 2021-11-07).

(2) Closing the Loop on the Plastics Dilemma: Proceedings of a Workshop-in brief, National Academies of Sciences, Engineering, and Medicine. The National Academies Press: Washington, DC, 2020.

(3) Scheutz, G. M.; Lessard, J. J.; Sims, M. B.; Sumerlin, B. S. Adaptable crosslinks in polymeric materials: Resolving the intersection of thermoplastics and thermosets. *J. Am. Chem. Soc.* **2019**, *141*, 16181−16196.
(4) Garcia, M. J.; Robertson, L. M. The future of plastics recycling. *Science* **2017**, *358*, 870−872.
(5) Hillmyer, M. A. The promise of plastics from plants. *Science* **2017**, *358*, 868−870.
(6) Zhu, Y.; Romain, C.; Williams, C. K. Sustainable polymers from renewable resources. *Nature* **2016**, *540*, 354−362.
(7) Zhang, X.; Fevre, M.; Jones, G. O.; Waymouth, R. M. Catalysis as an enabling science for sustainable polymers. *Chem. Rev.* **2018**, *118*, 839−885.
(8) Rorrer, N. A.; Nicholson, S.; Carpenter, A.; Biddy, M. J.; Grundl, N. J.; Beckham, G. T. Combining reclaimed PET with bio-based monomers enables plastics upcycling. *Joule* **2019**, *3*, 1006−1027.
(9) Yoshida, S.; Hiraga, K.; Takehana, T.; Taniguchi, I.; Yamaji, H.; Maeda, Y.; Toyohara, K.; Miyamoto, K.; Kimura, Y.; Oda, K. A bacterium that degrades and assimilates poly(ethylene terephthalate). *Science* **2016**, *351*, 1196−1199.
(10) Tournier, V.; Topham, C. M.; Gilles, A.; David, B.; Folgoas, C.; Moya-Leclair, E.; Kamionka, E.; Desrousseaux, M. L.; Texier, H.; Gavalda, S.; Cot, M.; Guémard, E.; Dalibey, M.; Nomme, J.; Cioci, G.; Barbe, S.; Chateau, M.; André, I.; Duquesne, S.; Marty, A. An engineered PET depolymerase to break down and recycle plastic bottles. *Nature* **2020**, *580*, 216−219.
(11) Jia, X.; Qin, C.; Friedberger, T.; Guan, Z.; Huang, Z. Efficient and selective degradation of polyethylenes into liquid fuels and waxes under mild conditions. *Sci. Adv.* **2016**, *2*, e1501591.
(12) Rahimi, A.; García, J. M. Chemical recycling of waste plastics for new materials production. *Nat. Rev. Chem.* **2017**, *1*, 0046.
(13) Häußler, M.; Eck, M.; Rothauer, D.; Mecking, S. Closed-loop recycling of polyethylene-like materials. *Nature* **2021**, *590*, 423−427.
(14) Baur, M.; Lin, F.; Morgen, T. O.; Odenwald, L.; Mecking, S. Polyethylene materials with in-chain ketones from nonalternating catalytic copolymerization. *Science* **2021**, *374*, 604−607.
(15) Jambeck, J. R.; Geyer, R.; Wilcox, C.; Siegler, T. R.; Perryman, M.; Andrady, A.; Narayan, R.; Law, K. L. Plastic waste inputs from land into the ocean. *Science* **2015**, *347*, 768−771.
(16) Geyer, R.; Jambeck, J. R.; Law, K. L. Production, use, and fate of all plastics ever made. *Sci. Adv.* **2017**, *3*, e1700782.
(17) The New Plastics Economy: Rethinking the Future of Plastics. https://ellenmacarthurfoundation.org/the-new-plastics-economy-rethinking-the-future-of-plastics (2016, accessed 2021-11-07). World Economic Forum, Ellen MacArthur Foundation and McKinsey & Company.
(18) Borrelle, S. B.; Ringma, J.; Law, K. L.; Monnahan, C. C.; Lebreton, L.; McGivern, A.; Murphy, E.; Jambeck, J.; Leonard, G. H.; Hilleary, M. A.; Eriksen, M.; Possingham, H. P.; De Frond, H.; Gerber, L. R.; Polidoro, B.; Tahir, A.; Bernard, M.; Mallos, N.; Barnes, M.; Rochman, C. M. Predicted growth in plastic waste exceeds efforts to mitigate plastic pollution. *Science* **2020**, *369*, 1515−1518.
(19) MacArthur, E. Beyond plastic waste. *Science* **2017**, *358*, 843−843.
(20) Lamb, J. B.; Willis, B. L.; Fiorenza, E. A.; Couch, C. S.; Howard, R.; Rader, D. N.; True, J. D.; Kelly, L. A.; Ahmad, A.; Jompa, J.; Harvell, C. D. Plastic waste associated with disease on coral reefs. *Science* **2018**, *359*, 460−462.
(21) Schneiderman, D. K.; Hillmyer, M. A. 50th Anniversary Perspective: There is a great future in sustainable polymers. *Macromolecules* **2017**, *50*, 3733−3749.
(22) Lu, X.-B.; Liu, Y.; Zhou, H. Learning Nature: Recyclable monomers and polymers. *Chem.—Eur. J.* **2018**, *24*, 11255−11266.
(23) Jehanno, C.; Pérez-Madrigal, M. M.; Demarteau, J.; Sardon, H.; Dove, A. P. Organocatalysis for depolymerisation. *Polym. Chem.* **2019**, *10*, 172−186.
(24) Tang, X.; Chen, E. Y.-X. Toward infinitely recyclable plastics derived from renewable cyclic esters. *Chem.* **2019**, *5*, 284−312.
(25) Lloyd, E. M.; Lopez Hernandez, H.; Feinberg, A. M.; Yourdkhani, M.; Zen, E. K.; Mejia, E. B.; Sottos, N. R.; Moore, J. S.; White, S. R. Fully recyclable metastable polymers and composites. *Chem. Mater.* **2019**, *31*, 398−406.
(26) Kaitz, J. A.; Lee, O. P.; Moore, J. S. Depolymerizable polymers: Preparation, applications, and future outlook. *MRS Commun.* **2015**, *5*, 191−204.
(27) Christensen, P. R.; Scheuermann, A. M.; Loeffler, K. E.; Helms, B. A. Closed-loop. recycling of plastics enabled by dynamic covalent diketoenamine bonds. *Nat. Chem.* **2019**, *11*, 442−448.
(28) Garcia, J. M.; Jones, G. O.; Virwani, K.; McCloskey, B. D.; Boday, D. J.; ter Huurne, G. M.; Horn, H. W.; Coady, D. J.; Bintaleb, A. M.; Alabdulrahman, A. M. S.; Alsewailem, F.; Almegren, H. A. A.; Hedrick, J. L. Recyclable, strong thermosets and organogels via paraformaldehyde condensation with diamines. *Science* **2014**, *344*, 732−735.
(29) Schneiderman, D. K.; Vanderlaan, M. E.; Mannion, A. M.; Panthani, T. R.; Batiste, D. C.; Wang, J. Z.; Bates, F. S.; Macosko, C. W.; Hillmyer, M. A. Chemically recyclable biobased polyurethanes. *ACS Macro. Lett.* **2016**, *5*, 515−518.
(30) Diesendruck, C. E.; Peterson, G. I.; Kulik, H. J.; Kaitz, J. A.; Mar, B. D.; May, P. A.; White, S. R.; Martínez, T. J.; Boydston, A. J.; Moore, J. S. Mechanically triggered heterolytic unzipping of a low-ceiling-temperature polymer. *Nat. Chem.* **2014**, *6*, 623−628.
(31) Abel, B. A.; Snyder, R. L.; Coates, G. W. Chemically recyclable thermoplastics from reversible-deactivation polymerization of cyclic acetals. *Science* **2021**, *373*, 783−789.
(32) Hong, M.; Chen, E. Y.-X. Chemically recyclable polymers: a circular economy approach to sustainability. *Green Chem.* **2017**, *19*, 3692−3706.
(33) Hong, M.; Chen, E. Y.-X. Future Directions for Sustainable Polymers. *Trends Chem.* **2019**, *1*, 148−151.
(34) Coates, G. W.; Getzler, Y. D. Y. L. Chemical recycling to monomer for an ideal, circular polymer economy. *Nat. Rev. Mater.* **2020**, *5*, 501−516.
(35) Cywar, R. M.; Rorrer, N. A.; Hoyt, C. B.; Beckham, G. T.; Chen, E. Y. X. Bio-based polymers with performance-advantaged properties. *Nat. Rev. Mater.* **2021**, DOI: 10.1038/s41578-021-00363-3.
(36) Shi, C.; Reilly, L. T.; Phani Kumar, V. S.; Coile, M. W.; Nicholson, S. R.; Broadbelt, L. J.; Beckham, G. T.; Chen, E. Y.-X. Design principles for intrinsically circular polymers with tunable properties. *Chem.* **2021**, *7*, 2896−2912.
(37) Olsén, P.; Odelius, K.; Albertsson, A.-C. Thermodynamic presynthetic considerations for ring-opening polymerization. *Biomacromolecules* **2016**, *17*, 699−709.
(38) Schneiderman, D. K.; Hillmyer, M. A. Aliphatic polyester block polymer design. *Macromolecules* **2016**, *49*, 2419−2428.
(39) Matyjaszewski, K. Architecturally Complex Polymers with Controlled Heterogeneity. *Science* **2011**, *333*, 1104−1105.
(40) Venkataraman, S.; Ng, V. W. L.; Coady, D. J.; Horn, H. W.; Jones, G. O.; Fung, T. S.; Sardon, H.; Waymouth, R. M.; Hedrick, J. L.; Yang, Y. Y. A Simple and Facile Approach to Aliphatic N-Substituted Functional Eight-Membered Cyclic Carbonates and Their Organocatalytic Polymerization. *J. Am. Chem. Soc.* **2015**, *137*, 13851−13860.
(41) Tang, X.; Hong, M.; Falivene, L.; Caporaso, L.; Cavallo, L.; Chen, E. Y.-X. The Quest for Converting Biorenewable Bifunctional alpha-Methylene-gamma-butyrolactone into Degradable and Recyclable Polyester: Controlling Vinyl-Addition/Ring-Opening/Cross-Linking Pathways. *J. Am. Chem. Soc.* **2016**, *138*, 14326−14337.
(42) Nuyken, O.; Pask, S. D. Ring-Opening Polymerization—An Introductory Review. *Polymers* **2013**, *5*, 361−403.
(43) Duda, A.; Kowalski, A. In *Handbook of Ring-Opening Polymerization*; Dubois, P., Coulembier, O., Raquez, J.-M., Eds.; Wiley-VCH: 2009; Chapter 1, pp 1−51.
(44) Becker, G.; Wurm, F. R. Functional biodegradable polymers via ring-opening polymerization of monomers without protective groups. *Chem. Soc. Rev.* **2018**, *47*, 7739−7782.

(45) Tian, H.; Tang, Z.; Zhuang, X.; Chen, X.; Jing, X. Biodegradable synthetic polymers: Preparation, functionalization and biomedical application. *Prog. Polym. Sci.* **2012**, *37*, 237−280.
(46) Seyednejad, H.; Ghassemi, A. H.; van Nostrum, C. F.; Vermonden, T.; Hennink, W. E. Functional aliphatic polyesters for biomedical and pharmaceutical applications. *J. Controlled Release* **2011**, *152*, 168−176.
(47) Hong, M.; Chen, E. Y.-X. Completely recyclable biopolymers with linear and cyclic topologies via ring-opening polymerization of γ-butyrolactone. *Nat. Chem.* **2016**, *8*, 42−49.
(48) Zhu, J.-B.; Watson, E. M.; Tang, J.; Chen, E. Y.-X. A synthetic polymer system with repeatable chemical recyclability. *Science* **2018**, *360*, 398−403.
(49) Zhu, J.-B.; Chen, E. Y.-X. Catalyst-Sidearm-Induced Stereoselectivity Switching in Polymerization of a Racemic Lactone for Stereocomplexed Crystalline Polymer with a Circular Life Cycle. *Angew. Chem., Int. Ed.* **2019**, *58*, 1178−1182.
(50) Shi, C.; Li, Z.-C.; Caporaso, L.; Cavallo, L.; Falivene, L.; Chen, E. Y.-X. Hybrid monomer design for unifying conflicting polymerizability, recyclability, and performance properties. *Chem.* **2021**, *7*, 670−685.
(51) Worch, J. C.; Dove, A. P. Harnessing polymers near equilibrium for better recycling. *Chem.* **2021**, *7*, 547−549.
(52) MacDonald, J. P.; Shaver, M. P. An aromatic/aliphatic polyester prepared via ring-opening polymerisation and its remarkably selective and cyclable depolymerisation to monomer. *Polym. Chem.* **2016**, *7*, 553−559.
(53) Lizundia, E.; Makwana, V. A.; Larrañaga, A.; Vilas, J. L.; Shaver, M. P. Thermal, structural and degradation properties of an aromatic−aliphatic polyester built through ring-opening polymerisation. *Polym. Chem.* **2017**, *8*, 3530−3538.
(54) Shi, C.-X.; Guo, Y.-T.; Wu, Y.-H.; Li, Z.-Y.; Wang, Y.-Z.; Du, F.-S.; Li, Z.-C. Synthesis and controlled organobase-catalyzed ring-opening polymerization of morpholine-2,5-dione derivatives and monomer recovery by acid-catalyzed degradation of the polymers. *Macromolecules* **2019**, *52*, 4260−4269.
(55) Yuan, J.; Xiong, W.; Zhou, X.; Zhang, Y.; Shi, D.; Li, Z.; Lu, H. 4-hydroxyproline-derived sustainable polythioesters: Controlled ring-opening polymerization, complete recyclability, and facile functionalization. *J. Am. Chem. Soc.* **2019**, *141*, 4928−4935.
(56) Shi, C.; McGraw, M. L.; Li, Z.-C.; Cavallo, L.; Falivene, L.; Chen, E. Y.-X. High-Performance Pan-Tactic Polythioesters with Intrinsic Crystallinity and Chemical Recyclability. *Sci. Adv.* **2020**, *6*, eabc0495.
(57) Xiong, W.; Chang, W.; Shi, D.; Yang, L.; Tian, Z.; Wang, H.; Zhang, Z.; Zhou, X.; Chen, E.-Q.; Lu, H. Geminal dimethyl substitution enables controlled polymerization of penicillamine-derived β-thiolactones and reversed depolymerization. *Chem.* **2020**, *6*, 1831−1843.
(58) Liu, Y.; Zhou, H.; Guo, J.-Z.; Ren, W.-M.; Lu, X.-B. Completely recyclable monomers and polycarbonate: approach to sustainable polymers. *Angew. Chem., Int. Ed.* **2017**, *56*, 4862−4866.
(59) Sanders, D. P.; Fukushima, K.; Coady, D. J.; Nelson, A.; Fujiwara, M.; Yasumoto, M.; Hedrick, J. L. A Simple and Efficient Synthesis of Functionalized Cyclic Carbonate Monomers Using a Versatile Pentafluorophenyl Ester Intermediate. *J. Am. Chem. Soc.* **2010**, *132*, 14724−14726.
(60) Yu, W.; Maynard, E.; Chiaradia, V.; Arno, M. C.; Dove, A. P. Aliphatic Polycarbonates from Cyclic Carbonate Monomers and Their Application as Biomaterials. *Chem. Rev.* **2021**, *121*, 10865−10907.
(61) Novak, B. M.; Grubbs, R. H. The ring opening metathesis polymerization of 7-oxabicyclo[2.2.1]hept-5-ene derivatives: a new acyclic polymeric ionophore. *J. Am. Chem. Soc.* **1988**, *110*, 960−961.
(62) Schrock, R. R. Living ring-opening metathesis polymerization catalyzed by well-characterized transition-metal alkylidene complexes. *Acc. Chem. Res.* **1990**, *23*, 158−165.
(63) Bielawski, C. W.; Grubbs, R. H. Highly Efficient Ring-Opening Metathesis Polymerization (ROMP) Using New Ruthenium Catalysts Containing N-Heterocyclic Carbene Ligands. *Angew. Chem., Int. Ed.* **2000**, *39*, 2903−2906.
(64) Ogba, O. M.; Warner, N. C.; O'Leary, D. J.; Grubbs, R. H. Recent advances in ruthenium-based olefin metathesis. *Chem. Soc. Rev.* **2018**, *47*, 4510−4544.
(65) Grubbs, R. B.; Grubbs, R. H. 50th Anniversary Perspective: Living Polymerization—Emphasizing the Molecule in Macromolecules. *Macromolecules* **2017**, *50*, 6979−6997.
(66) Sathe, D.; Zhou, J.; Chen, H.; Su, H.-W.; Xie, W.; Hsu, T.-G.; Schrage, B. R.; Smith, T.; Ziegler, C. J.; Wang, J. Olefin metathesis-based chemically recyclable polymers enabled by fused-ring monomers. *Nat. Chem.* **2021**, *13*, 743−750.
(67) Chen, H.; Shi, Z.; Hsu, T.-G.; Wang, J. Overcoming the Low Driving Force in Forming Depolymerizable Polymers through Monomer Isomerization. *Angew. Chem., Int. Ed.* **2021**, *60*, 25493−25498.
(68) Ofstead, E. A.; Calderon, N. Equilibrium ring-opening polymerization of mono- and multicyclic unsaturated monomers. *Makromol. Chem.* **1972**, *154*, 21−34.
(69) Monfette, S.; Fogg, D. E. Equilibrium Ring-Closing Metathesis. *Chem. Rev.* **2009**, *109*, 3783−3816.
(70) Hejl, A.; Scherman, O. A.; Grubbs, R. H. Ring-Opening Metathesis Polymerization of Functionalized Low-Strain Monomers with Ruthenium-Based Catalysts. *Macromolecules* **2005**, *38*, 7214−7218.
(71) Tuba, R.; Grubbs, R. H. Ruthenium catalyzed equilibrium ring-opening metathesis polymerization of cyclopentene. *Polym. Chem.* **2013**, *4*, 3959−3962.
(72) Tuba, R.; Al-Hashimi, M.; Bazzi, H. S.; Grubbs, R. H. One-Pot Synthesis of Poly(vinyl alcohol) (PVA) Copolymers via Ruthenium Catalyzed Equilibrium Ring-Opening Metathesis Polymerization of Hydroxyl Functionalized Cyclopentene. *Macromolecules* **2014**, *47*, 8190−8195.
(73) Liu, H.; Nelson, A. Z.; Ren, Y.; Yang, K.; Ewoldt, R. H.; Moore, J. S. Dynamic Remodeling of Covalent Networks via Ring-Opening Metathesis Polymerization. *ACS Macro Lett.* **2018**, *7*, 933−937.
(74) Neary, W. J.; Kennemur, J. G. Polypentenamer Renaissance: Challenges and Opportunities. *ACS Macro Lett.* **2019**, *8*, 46−56.
(75) Neary, W. J.; Isais, T. A.; Kennemur, J. G. Depolymerization of Bottlebrush Polypentenamers and Their Macromolecular Metamorphosis. *J. Am. Chem. Soc.* **2019**, *141*, 14220−14229.
(76) Feist, J. D.; Xia, Y. Enol Ethers Are Effective Monomers for Ring-Opening Metathesis Polymerization: Synthesis of Degradable and Depolymerizable Poly(2,3-dihydrofuran). *J. Am. Chem. Soc.* **2020**, *142*, 1186−1189.
(77) Choi, T.-L.; Lee, C. W.; Chatterjee, A. K.; Grubbs, R. H. Olefin Metathesis Involving Ruthenium Enoic Carbene Complexes. *J. Am. Chem. Soc.* **2001**, *123*, 10417−10418.
(78) Song, A.; Parker, K. A.; Sampson, N. S. Synthesis of Copolymers by Alternating ROMP (AROMP). *J. Am. Chem. Soc.* **2009**, *131*, 3444−3445.
(79) Fomine, S.; Tlenkopatchev, M. A. Ring-Opening of Cyclohexene via Metathesis by Ruthenium Carbene Complexes. A Computational Study. *Organometallics* **2007**, *26*, 4491−4497.
(80) Hlil, A. R.; Balogh, J.; Moncho, S.; Su, H.-L.; Tuba, R.; Brothers, E. N.; Al-Hashimi, M.; Bazzi, H. S. Ring opening metathesis polymerization (ROMP) of five- to eight-membered cyclic olefins: Computational, thermodynamic, and experimental approach. *J. Polym. Sci., Part A: Polym. Chem.* **2017**, *55*, 3137−3145.
(81) Song, A.; Parker, K. A.; Sampson, N. S. Cyclic Alternating Ring-Opening Metathesis Polymerization (CAROMP). Rapid Access to Functionalized Cyclic Polymers. *Org. Lett.* **2010**, *12*, 3729−3731.
(82) Romulus, J.; Tan, L.; Weck, M.; Sampson, N. S. Alternating Ring-Opening Metathesis Polymerization Copolymers Containing Charge-Transfer Units. *ACS Macro Lett.* **2013**, *2*, 749−752.
(83) Tan, L.; Parker, K. A.; Sampson, N. S. A Bicyclo[4.2.0]octene-Derived Monomer Provides Completely Linear Alternating Copolymers via Alternating Ring-Opening Metathesis Polymerization (AROMP). *Macromolecules* **2014**, *47*, 6572−6579.

https://doi.org/10.1021/jacs.1c12278
J. Am. Chem. Soc. 2022, 144, 2264−2275

(84) Tan, L.; Li, G.; Parker, K. A.; Sampson, N. S. Ru-Catalyzed Isomerization Provides Access to Alternating Copolymers via Ring-Opening Metathesis Polymerization. *Macromolecules* **2015**, *48*, 4793−4800.
(85) Elling, B. R.; Xia, Y. Living Alternating Ring-Opening Metathesis Polymerization Based on Single Monomer Additions. *J. Am. Chem. Soc.* **2015**, *137*, 9922−9926.
(86) Elling, B. R.; Su, J. K.; Xia, Y. Degradable Polyacetals/Ketals from Alternating Ring-Opening Metathesis Polymerization. *ACS Macro Lett.* **2020**, *9*, 180−184.
(87) Elling, B. R.; Su, J. K.; Xia, Y. Polymerization of Cyclopropenes: Taming the Strain for the Synthesis of Controlled and Sequence-Regulated Polymers. *Acc. Chem. Res.* **2021**, *54*, 356−365.
(88) Peterson, G. I.; Choi, T.-L. Cascade polymerizations: recent developments in the formation of polymer repeat units by cascade reactions. *Chem. Sci.* **2020**, *11*, 4843−4854.
(89) Park, H.; Kang, E.-H.; Müller, L.; Choi, T.-L. Versatile Tandem Ring-Opening/Ring-Closing Metathesis Polymerization: Strategies for Successful Polymerization of Challenging Monomers and Their Mechanistic Studies. *J. Am. Chem. Soc.* **2016**, *138*, 2244−2251.
(90) Lee, H.-K.; Lee, J.; Kockelmann, J.; Herrmann, T.; Sarif, M.; Choi, T.-L. Superior Cascade Ring-Opening/Ring-Closing Metathesis Polymerization and Multiple Olefin Metathesis Polymerization: Enhancing the Driving Force for Successful Polymerization of Challenging Monomers. *J. Am. Chem. Soc.* **2018**, *140*, 10536−10545.
(91) Sui, X.; Zhang, T.; Pabarue, A. B.; Fu, L.; Gutekunst, W. R. Alternating Cascade Metathesis Polymerization of Enynes and Cyclic Enol Ethers with Active Ruthenium Fischer Carbenes. *J. Am. Chem. Soc.* **2020**, *142*, 12942−12947.
(92) Park, H.; Choi, T.-L. Fast Tandem Ring-Opening/Ring-Closing Metathesis Polymerization from a Monomer Containing Cyclohexene and Terminal Alkyne. *J. Am. Chem. Soc.* **2012**, *134*, 7270−7273.
(93) McGuire, T. M.; Pérale, C.; Castaing, R.; Kociok-Köhn, G.; Buchard, A. Divergent Catalytic Strategies for the Cis/Trans Stereoselective Ring-Opening Polymerization of a Dual Cyclic Carbonate/Olefin Monomer. *J. Am. Chem. Soc.* **2019**, *141*, 13301−13305.
(94) Pratt, R. C.; Lohmeijer, B. G. G.; Long, D. A.; Waymouth, R. M.; Hedrick, J. L. Triazabicyclodecene: A simple bifunctional organocatalyst for acyl transfer and ring-opening Polymerization of cyclic esters. *J. Am. Chem. Soc.* **2006**, *128*, 4556−4557.
(95) Zhang, X.; Jones, G. O.; Hedrick, J. L.; Waymouth, R. M. Fast and selective ring-opening polymerizations by alkoxides and thioureas. *Nat. Chem.* **2016**, *8*, 1047−1053.
(96) Chuma, A.; Horn, H. W.; Swope, W. C.; Pratt, R. C.; Zhang, L.; Lohmeijer, B. G. G.; Wade, C. G.; Waymouth, R. M.; Hedrick, J. L.; Rice, J. E. The reaction mechanism for the organocatalytic ring-opening polymerization of l-lactide using a guanidine-based catalyst: Hydrogen-bonded or covalently bound? *J. Am. Chem. Soc.* **2008**, *130*, 6749−6754.
(97) Tang, X.; Chen, E. Y.-X. Chemical synthesis of perfectly isotactic and high melting bacterial poly(3-hydroxybutyrate) from bio-sourced racemic cyclic diolide. *Nat. Commun.* **2018**, *9*, 2345.
(98) Tang, X.; Westlie, A. H.; Watson, E. M.; Chen, E. Y.-X. Stereosequenced crystalline polyhydroxyalkanoates from diastereomeric monomer mixtures. *Science* **2019**, *366*, 754−758.
(99) Carpentier, J.-F. Rare-Earth Complexes Supported by Tripodal Tetradentate Bis(phenolate) Ligands: A Privileged Class of Catalysts for Ring-Opening Polymerization of Cyclic Esters. *Organometallics* **2015**, *34*, 4175−4189.
(100) Jaffredo, C. G.; Chapurina, Y.; Guillaume, S. M.; Carpentier, J.-F. From Syndiotactic Homopolymers to Chemically Tunable Alternating Copolymers: Highly Active Yttrium Complexes for Stereoselective Ring-Opening Polymerization of *β*-Malolactonates. *Angew. Chem., Int. Ed.* **2014**, *53*, 2687−2691.

https://doi.org/10.1021/jacs.1c12278
J. Am. Chem. Soc. 2022, 144, 2264−2275